Next generation integrated drive: A novel thermal and electrical integration technique for high power density converters used in automotive drive systems

B. Ahmadi, J. Espina, L. de Lillo, R. Abebe, L. Empringham, C.M. Johnson

**PEMC group, Department of Electrical and Electronic engineering, The University of Nottingham, UK,*
lee.empringham@nottingham.ac.uk, mark.johnson@nottingham.ac.uk

Keywords: High power density converters, Integrated drive, MOSFET power modules, Sintering, Cooling system.

Abstract

In this paper, an innovative method of electro-thermal integration of a drive system is presented. Important challenges of this integration consist of, firstly coupled thermal design of switching power modules and PM electric motor and secondly integration of high frequency switching devices into the motor housing, without compromising the performance of these transistors. To provide a solution to these challenges, an integrated liquid cooling system for both stator windings and transistor modules is designed. On the other hand, a specific power module is designed to meet the specific requirements of this packaging technique.

1 Introduction

Recent developments in energy storage technologies have made the *all-electric vehicle* concept more attractive to the automotive industry [1]. Higher energy density batteries combined with highly efficient variable speed motor drives, pictured a new perspective of higher electric range vehicles [2].

Electric propulsion systems implemented in the *all-electric vehicle*s, still need to achieve a higher degree of power density to meet the requirements of this industry. One of the paths to attain this goal is direct liquid cooling of the stator windings [3][4], which allows higher current densities in the windings and therefore can push the frontiers of the achievable power densities. In this regard, thermal models are also developed to optimise the design and explore the maximum current density in the stator windings [5], [6]. Another path is eliminating the connections and wires between the power electronic drive system and the electric motor. Integrating DC bus bars and discrete switching devices in the motor housing is one of the proposed solutions [7]. This technique can help to reduce the EMI problems and reduce the effect of switching noises on other parts of electric vehicle.

On the other hand, this integrated drive concept creates new challenges in various design aspects. First of all, proximity of the switching devices to the motor casing implies that the thermal aspects of the two systems are tightly coupled to each other. Secondly, by using wide band-gap semiconductors, which are optimised to operate at high switching frequencies, proper design of the integrated switching circuit becomes a determining factor. An optimised design can enable us to totally explore the advantages of these devices and to increase the power density of this integrated power electronic drive. Finally, new thoughts are required for designing mechanical aspects, electrical connections and assembly of the whole system.

In this paper, a novel method of structural integration of a power electronic converter into a permanent magnet motor casing is presented. In this method, power modules and stator windings share the same coolant liquid. Power modules are directly assembled in the motor housing and are connected to the stator windings, though a novel multilayer PCB structure. On the other hand, control hardware and gate driver circuits are also integrated into the same space, close to the power modules. This paper emphasises on the integration of power electronic hardware, the design of electric motor is covered in a separate paper.

2 Overview of the system

A general overview of this integrated drive system is presented in Figure-1. 3 phase salient permanent magnet motor designed for this application consists of 3 separate

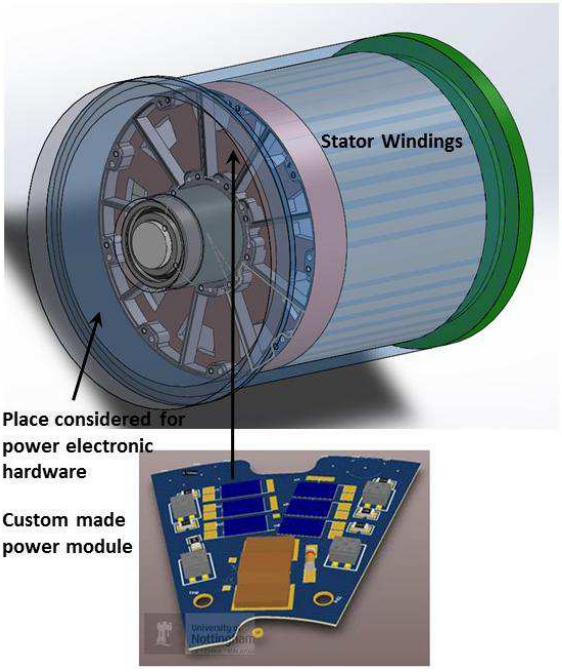

Figure-1: Representation of the PM motor and integration of the switching modules into the motor housing

3phase sub-machines. The nominal power of the designed motor is 80 kW at 30000 rpm. At this nominal power, current level flowing through the stator windings is 105 Arms. In the designed stator, this current level is equivalent to a density of 28 A/mm^2 in the windings. Consequently, windings are thermally managed by direct liquid cooling method. The same coolant, which is de-ionised water, is flowing through the power modules cooling system. This will be explained in section 2. Each winding set is connected to one power module through an innovative multi-layer PCB.

1 Controller hardware

Each sub-machine has its own control hardware to manage the high speed control, generating PWM vectors and fast protection functions. A higher level supervisory system provides the speed and torque control and other supervisory functions.

Figure-2 explains a schematic representation of the control hardware and the designed PCBs are shown in Figure-3. The first layer, from top is the Master controller board consisting of a Texas instrument TMS320F28379D microcontroller and a Microsemi iGLOO2 FPGA. This Master board is connected to 3 local controller boards (auxiliary board) though a 22 MHz customised SPI connection and 4 quantities will be sending to each: rotor speed ω_s, electrical angle ϑ_e, stator frame current i_α and i_β. These quantities will be available to local controllers at the beginning of each switching cycle (60 kHz).

The second boards from top are auxiliary boards with the same structure as the Master board (µ-controller and FPGA). Four integrated ADC of the µ-controllers are used to make a synchronous measurement of 3 phase currents and local DC bus voltages. These 16-bit data will be sending once per switching cycle and will be received by Master after one cycle.

A vector space calculator is implemented in 3 local µ-controllers (for each sub-machine). PWM waveforms will be generated by FPGAs and be sending to gated driver boards through high speed differential lines. Details on the control strategies and software are provided in another paper.

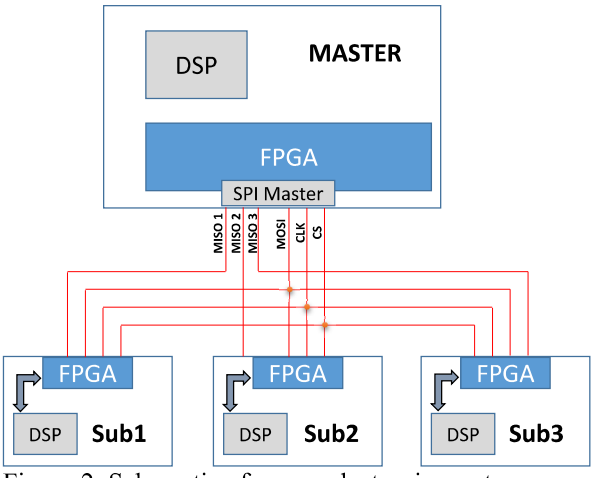

Figure-2: Schematic of power electronics system

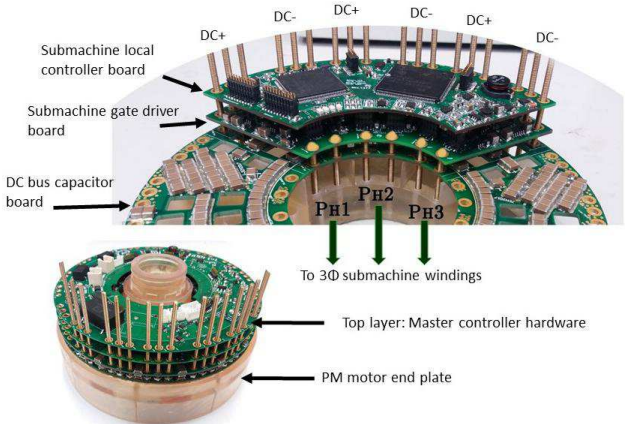

Figure-3: Power electronic hardware integrated into the PM motor housing

2 Gate driver integration

Cross section of different layers from Master controller board to the stator windings is represented in Figure-4. A DC bus capacitor board is placed just next to the power modules and gate driver board. Placing this 37µF, X7R capacitor board in few mm of the switching module will reduce the EMI noises considerably.

The physical distance between the gate driver boards and the power modules is less than 8mm. This short distance will prevent oscillations on the gate signals. A 3 W custom made gate driver is designed for each phase to switch 3 parallel Silicon Carbide transistors at 60 kHz.

The connections between the external DC source and capacitor board are provided through brass vertical bars.

3 Integrated power module design

Each power module consists of 6 SiC MOSFETs (2×3 in parallel) transistors (1.2 kV) sintered on a AlN substrate. Gate resistors, current measurement shunt resistor as well as a decoupling capacitor are also included on this substrate (Figure-1). Source and gate contacts are on top side of the 7.3×4.35 mm transistor die and collector contact is on back

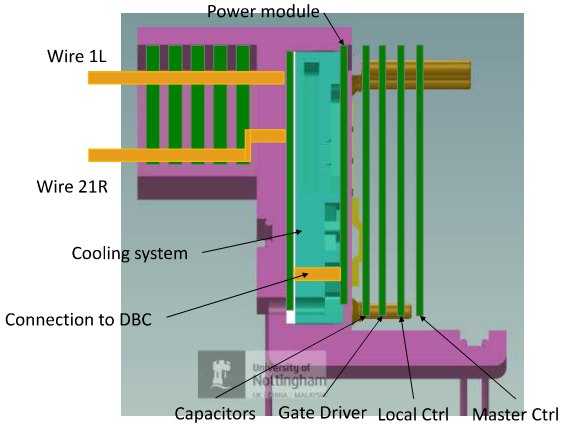

Figure-4: Connection of the power modules to the windings and rest of the system.

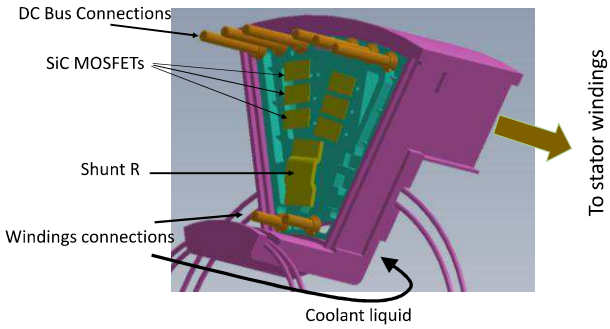

Figure-5: Details of the power module, placed in the motor endplate.

side. Transistors are first sintered on a flex PCB using an organic die attach paste to provide access to gate and source contacts. The ensemble of transistors and flex PCB is then sintered back onto the ALN substrate, to complete the module connections. DC bus connections are the same brass bars, as described in previous section. These brass bars are directly soldered onto the AlN substrate and connect them to decoupling capacitor board and main DC source (Figure-4). This method is an enhanced version of the one presented in [8] to improve the reliability of the contacts.

The cooling system is placed on the back side of AlN substrate, as shown in Figure-5. Connection to the windings is provided via a multi later PCB design. U-shape stator windings are closed by a special arrangement of PCBs, placed at the end of these u-shape wires. The first and the last turns of 21 stator winding turns will be going through all the PCB layers. These two connections will be passing through the cooling system, underneath of the substrates, and finally be terminating into the power module via two small brass bars.

Stator windings are immersed in liquid and the power module's cooling system shares the same liquid as shown in Figure-5. Coolant liquid, coming through the outer circumference of rotor shaft, is being sprayed behind the DBC to cool down the power module.

Cross section of the liquid guide, placed at the back side of the AlN substrates is shown in Figure-6. This solution is based on direct substrate cooling method with targeted impingement which can provide a very low specific thermal resistance [9]. The inlet of the coolant liquid can be seen in the cut made in this image. The liquid follows into the provided channel and is being sprayed out from the holes placed behind the transistor dies. The liquid then continues its path, through the wide opening, to the stator windings. It will circulate around the end winding PCBs and finally finds its way to the stator windings.

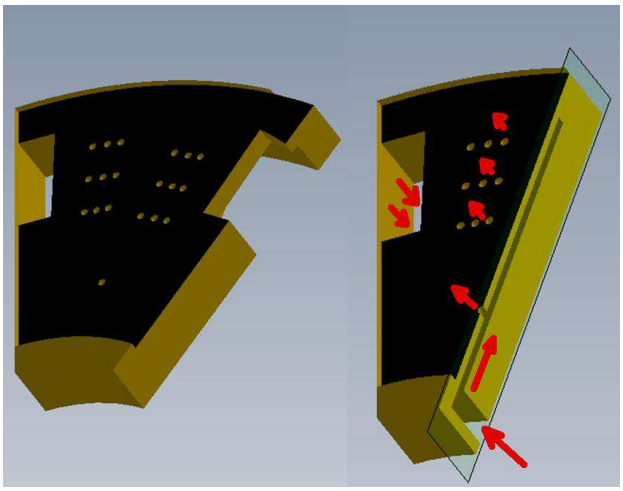

Figure-6: Liquid guide placed at the back side of the power module substrate.

4 Finite elements simulation of the integrated cooling system

In order to evaluate the validity of the proposed integrated design, the power module cooling system and junctions to the stator circuit, are modelled in computational fluid dynamic software (ANSYS Fluent).

In these simulations, an aqueous solution of ethylene-glycol (50% weight) is selected as coolant liquid. Thermal properties of this liquid are summarised inTable-1. Although these properties depend on temperature, their variation ranges are small (except for viscosity) and values for 110 °C are considered for these simulations.

First simulation is set for a constant temperature of 110 °C to verify circulation of the coolant liquid in the designed liquid guide.

The result of the simulation is shown in Figure-7. The flow rate is considered as 50 ml/s for this simulation. The cross section of the inlet opening is about 35 mm^2 and this flow rate is considered in order to minimise the presseure drop in the coolant liquid circuit, as this circuit is supposed to be applicable in automative industry. In this simulation the pressure drop between inlet and outlet (to the stator windings) is 0.03 bars.

One can notice that the velocity is higher just after the inlet knee (under the shunt resistor) and also in the regions where the liquide is being sprayed onto the back of the power module. It can be concluded that at these regions the pressure of the liquide is being increased, the fact that will help to

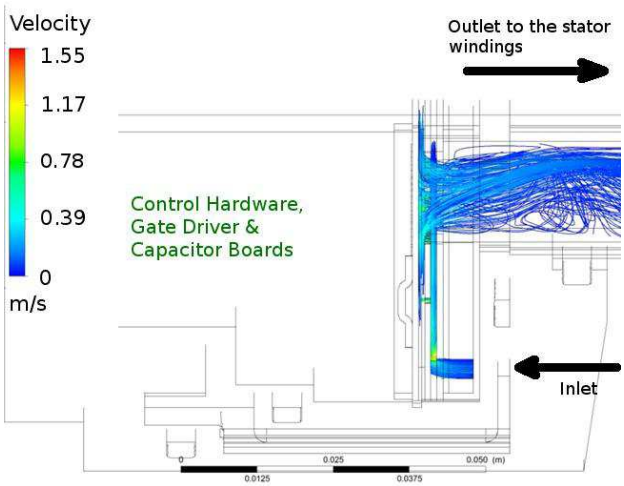

Figure-7: Simulated velocity of the coolant liquid (water-glycol 50%).

°C	Specific gravity	Specific Heat kJ/kg K^{-1}	Thermal conductivity mw/m K^{-1}	Viscosity g/m s^{-1}
110	1	3.75	33.5	0.6
70	1.04	3.63	34.4	1.1
30	1.08	3.50	34.7	2.5

Table-1: Thermal properties of 50% wt. aqueous solution of ethylene-glycol at 3 different temperatures.

increase the thermal heat exchange between the substrate and the coolant liquid.

These results show that the designed liquid guide can efficiently impinge the fluid into fine droplets, which in turn will enhance the cooling function .

In order to investigate the effect of viscosity (wich decreases with temperature) other simulations with higher viscosity values up to 10 g/m.s^{-1} has beed analysed, however, there is no remarkable effect in the results.

In the second simulation, an estimated power loss is set for the transistors and the same conditions as the previous simulation is applied on the coolant circuit in order to obtain the steady state temperature of the dies. This simulation provide an estimation of the efficiency of the designed integrated cooling system.

At full rated power of the motor (80 kW) the sum of switching and conduction current (105 A in 3 parallel transistors) losses, is estimated at 400 W. This loss is then distributed evenly to all 6 transistors, and is inserted as 6 separate heat sources in the simulation. Figure-8 shows the temperature distribution on the substrate, seen from transistor side. This can be considered as junction temperature as the transistor dies are directly sintered onto the substrate. One can observe that the steady state temperature for full power is reaching the limits of the operation temperature (250 °C) for the employed organic paste die attach technique [10] and slightly more than acceptable operating temperature of these SiC transistors (175 °C). In these conditions, a more optimum

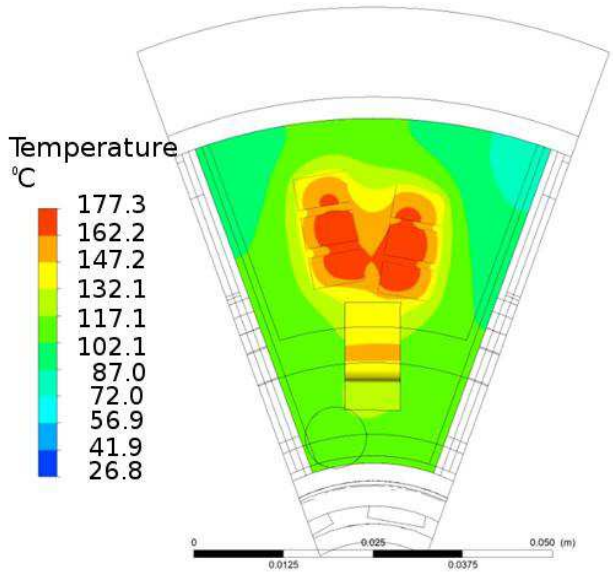

Figure-8: Simulated temperature obtained by coupled CFD/thermal simulation.

design of the coolant liquid guide and the choice of the coolant liquid need to be reconsidered.

5 Conclusion

In this paper, two important challenges for the next generation integrated drive have been addressed. The innovative integration technique, proposed in this paper aims to provide solutions in both domains of thermal and electrical integration of a drive system. In terms of electrical integration, several compact PCB boards have been designed to bring the controller hardware close to the gate drivers and switching modules. A switching module has been designed to fit into the endplate of a compact permanent magnet motor and to integrate into the stator windings. This highly compact electrical design, allowed implementing a new thermal design which incorporate both stator and power module cooling system. The finite element simulations show that the designed system can potentially provide an acceptable solution for the aimed rated power (80 kW).

Acknowledgements

This project has been funded by Engineering and Physical Sciences Research Council (EPSRC) National Centre for Power Electronics, UK.

References

[1] T. Placke, R. Kloepsch, S. Dühnen, and M. Winter, 'Lithium ion, lithium metal, and alternative rechargeable battery technologies: the odyssey for high energy density', *J. Solid State Electrochem.*, vol. 21, no. 7, pp. 1939–1964, Jul. 2017.

[2] M. S. Kumar and S. T. Revankar, 'Development scheme and key technology of an electric vehicle: An overview', *Renew. Sustain. Energy Rev.*, vol. 70, pp. 1266–1285, Apr. 2017.

[3] P. Lindh *et al.*, 'Direct Liquid Cooling Method verified with an Axial-Flux Permanent-Magnet Traction Machine Prototype', *IEEE Trans. Ind. Electron.*, pp. 1–1, 2017.

[4] Z. Huang, S. Nategh, V. Lassila, M. Alakula, and J. Yuan, 'Direct oil cooling of traction motors in hybrid drives', 2012, pp. 1–8.

[5] R. Camilleri, D. A. Howey, and M. D. McCulloch, 'Predicting the Temperature and Flow Distribution in a Direct Oil-Cooled Electrical Machine With Segmented Stator', *IEEE Trans. Ind. Electron.*, vol. 63, no. 1, pp. 82–91, Jan. 2016.

[6] S. Nategh, Z. Huang, A. Krings, O. Wallmark, and M. Leksell, 'Thermal Modeling of Directly Cooled Electric Machines Using Lumped Parameter and Limited CFD Analysis', *IEEE Trans. Energy Convers.*, vol. 28, no. 4, pp. 979–990, Dec. 2013.

[7] M. N. Anwar, M. Teimor, R. E. Luken, J. J. Brautigan, and I. Visteon Global Technologies, *Electric machine with integrated electronics in a circular/closed-loop arrangement*. 2004.

[8] J. Espina, B. Ahmadi, L. Empringham, L. D. Lillo, and M. Johnson, 'Highly-integrated power cell for high-power wide band-gap power converters', in *2017 IEEE 3rd International*

Future Energy Electronics Conference and ECCE Asia (IFEEC 2017 - ECCE Asia), 2017, pp. 146–150.
[9] C. M. Johnson, A. Castellazzi, R. Skuriat, P. Evans, J. Li, and P. Agyakwa, 'Integrated High Power Modules', in *2012 7th International Conference on Integrated Power Electronics Systems (CIPS)*, 2012, pp. 1–10.
[10] R. Khazaka, L. Mendizabal, D. Henry, and R. Hanna, 'Survey of High-Temperature Reliability of Power Electronics Packaging Components', *IEEE Trans. Power Electron.*, vol. 30, no. 5, pp. 2456–2464, May 2015.